A Cross-layer Optimized Receiver Design for Wireless Feedback Control Systems

Kentaro Kobayashi, *Member, IEEE,* Hiraku Okada, *Member, IEEE,* and Masaaki Katayama, *Senior Member, IEEE*

Abstract

In this paper, a cross-layer design for communication and control layers for wireless feedback control systems is considered, and an optimized receiver design for state feedback is proposed. The proposed receiver is designed on the basis of a maximum à posteriori probability decision and utilizes the control layer's information, namely, the estimated state information of a Kalman filter-based state observer, as the à priori information of the transmitted state feedback. In addition, the proposed receiver provides the error covariance information of the received state feedback for the control layer. The recursive structure of the receiver and state observer is simple and suitable for the feedback control loop. The improvement in the channel error probability is supported by the control accuracy and vice versa. Numerical results show that the proposed receiver can effectively reduce the number of channel errors in the received state feedback and improve the control performance.

Index Terms

Cross-layer design, optimum receiver, maximum à posteriori probability, state observer, networked control systems.

I. INTRODUCTION

WIRELESS networked control systems are feedback systems in which control loops are connected via wireless communication channels. Although wireless communication has several

This work is supported in part by Japan Society for the Promotion of Science (JSPS) Grant-in-Aid for Young Scientists (B) under Grant 15K21071. The authors would like to thank Prof. Takaya Yamazato of Nagoya University for his valuable suggestions.

Kentaro Kobayashi, Hiraku Okada, and Masaaki Katayama are with Institute of Materials and Systems for Sustainability, Nagoya University, Nagoya 464-8603, Japan (e-mail:kobayasi@nuee.nagoya-u.ac.jp).

advantages such as reconfigurability, mobility, and easy installation in places where cabling is difficult, there are some disadvantages, including data rate limitations, transmission delays, and channel errors, which cause deterioration in the control performance [1]. In previous studies, several types of controllers and state observers that consider channel errors to improve the control performance have been proposed. For example, Kalman filter-based state estimation schemes [2]–[5], linear quadratic optimal control schemes [5]–[8], predictive control schemes [9]–[12], and H_∞ control schemes [13]–[15] have been proposed for various control situations. The above studies focus on reducing the influence of channel errors from the viewpoint of a control layer. In contrast, in this paper, we focus on reducing the number of channel errors in control data packets from the viewpoint of a communication layer.

From the viewpoint of the communication layer designed for networked control systems, a cooperative communication scheme [16], a hybrid automatic repeat request scheme [17], an adaptive modulation scheme [18], an adaptive power management scheme [19], and adaptive forward error correction schemes [20], [21] have been proposed to reduce the number of channel errors. These studies are based on an attractive concept in which the communication layer utilizes the control layer's quality information and configures communication parameters to improve the performance of both the communication and control layers. In addition, cross-layer designs in the source and channel encoding of control data have been discussed in [22]–[24]. These studies have shown that the side information of the feedback and feedforward structures improves the encoding and decoding efficiencies. In [25], [26] a decoding scheme that utilizes the information of a state observer was presented to improve the channel error probability. However, since the employed state estimation does not consider channel errors and the actual error detection, it performs well for a high signal-to-noise ratio (SNR) but poorly for a low SNR compared to not using the state information.

The main contribution of this paper is a cross-layer design for the optimized receiver for state feedback in wireless feedback control systems. The proposed receiver utilizes the control layer's information as the à priori information of the transmitted state feedback and provides the error covariance information of the received state feedback to the control layer. Specifically, the proposed receiver is a maximum á posteriori probability (MAP)-based receiver that utilizes the estimated state information of a Kalman filter-based state observer as the à priori information of the transmitted state feedback. In addition, the proposed receiver provides the covariance matrix of the effect of undetected bit errors on the received state feedback for the state observer. The

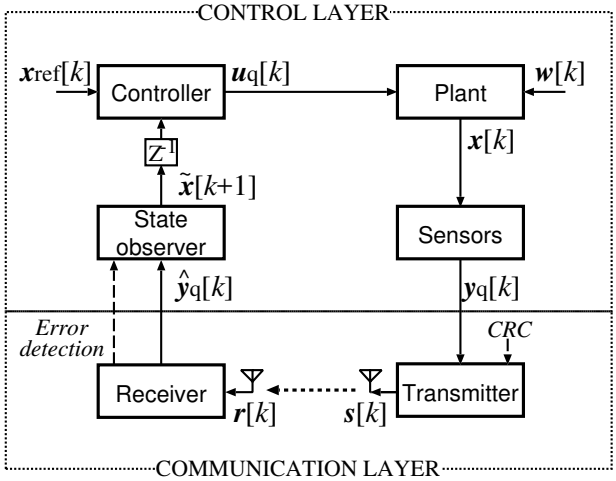

Fig. 1. Wireless feedback control system.

recursive structure of the receiver and state observer is simple and suitable for the feedback control loop. The improvement in the channel error probability of the receiver is supported by the accuracy of the state observer and vice versa; therefore, the proposed receiver can effectively reduce the number of channel errors in the received state feedback and improve the control performance, particularly at a low SNR.

The remainder of this paper is organized as follows. The system model of the considered wireless networked control system is described in Section II. The proposed receiver design is explained in detail in Section III. Numerical examples of the system performance are provided in Section IV and the conclusion of the study is presented in Section V.

II. System model

The considered wireless feedback control system is shown in Figure 1. The system is a feedback control system that wirelessly feeds the sensors' output back. The control layer of the system consists of a controller, state observer, plant, and set of sensors. The details of the control layer are explained in Section II-A. The communication layer of the system consists of a transmitter, wireless channel, and receiver. The details of the communication layer are explained in Section II-B.

A. Control layer

The structure of the control layer is a standard closed control loop. The plant's state ($\boldsymbol{x}[k]$) affected by a system disturbance ($\boldsymbol{w}[k]$) is controlled by an input signal ($\boldsymbol{u}_{\mathrm{q}}[k]$) calculated at the controller according to a reference state ($\boldsymbol{x}_{\mathrm{ref}}[k]$). The set of sensors observes the plant and reports an observed state ($\boldsymbol{y}_{\mathrm{q}}[k]$) to the state observer. The state observer estimates the plant's state from the received state ($\hat{\boldsymbol{y}}_{\mathrm{q}}[k]$) and passes the estimated plant state ($\tilde{\boldsymbol{x}}[k+1]$) to the controller. The controller calculates the next input signal according to the next reference signal and estimated plant state.

1) Plant: The plant is assumed to be linear time-invariant, and the discrete-time state-space model is expressed as

$$\boldsymbol{x}[k+1] = \boldsymbol{A}\boldsymbol{x}[k] + \boldsymbol{B}\boldsymbol{u}_{\mathrm{q}}[k] + \boldsymbol{w}[k], \tag{1}$$

where the state vector and quantized input vector of the plant at the time index $k(=0,1,2\ldots)$ with the sampling interval T_{s} are denoted as $\boldsymbol{x}[k] \in \mathbb{R}^{N_{\mathrm{x}}}$ and $\boldsymbol{u}_{\mathrm{q}}[k] \in \mathbb{R}^{N_{\mathrm{u}}}$, respectively. $\boldsymbol{A} \in \mathbb{R}^{N_{\mathrm{x}} \times N_{\mathrm{x}}}$ and $\boldsymbol{B} \in \mathbb{R}^{N_{\mathrm{x}} \times N_{\mathrm{u}}}$ are coefficient matrices that represent the plant. $\boldsymbol{w}[k] \in \mathbb{R}^{N_{\mathrm{x}}}$ is a system disturbance vector and assumed to be a white Gaussian random vector whose mean vector and covariance matrix are $\boldsymbol{0}$ and $\boldsymbol{W}$, respectively. $\mathbb{R}$ represents the real number field, and its superscript represents the dimension of a vector or matrix.

2) Sensors: At each time index, the set of sensors observes the plant and outputs $\boldsymbol{y}[k] \in \mathbb{R}^{N_{\mathrm{y}}}$. Using the output matrix $\boldsymbol{C} \in \mathbb{R}^{N_{\mathrm{y}} \times N_{\mathrm{x}}}$, which represents the observation of the plant's state, $\boldsymbol{y}[k]$ is represented as the linear transformation $\boldsymbol{y}[k] = \boldsymbol{C}\boldsymbol{x}[k]$. If $\boldsymbol{C}$ is a matrix that has only one "1" in each row and "0" for all other elements, it indicates that the sensors observe a part of the plant's state, i.e., $\boldsymbol{y}[k]$ consists of N_{y} of N_{x} elements of $\boldsymbol{x}[k]$.

Then, $\boldsymbol{y}[k]$ is transformed into $\boldsymbol{y}_{\mathrm{q}}[k] \in \mathbb{R}^{N_{\mathrm{y}}}$ via the analog-to-digital conversion and input into the communication layer, i.e., the transmitter. The conversion is assumed to be uniform quantization, which is widely used as a model of the analog-to-digital conversion, and the analysis of the mean squared distortion of its quantized values with channel errors has been presented in [27]. Here, L-bit uniform quantization is used, and each vector element of $\boldsymbol{y}_{\mathrm{q}}[k]$ is quantized as an L-bit digital value; to simplify the notation, mid-tread type quantization and the same bit length are used for all vector elements.

In this case, the relationship between $\boldsymbol{y}_{\mathrm{q}}[k]$ and $\boldsymbol{y}[k]$ can be represented as $\boldsymbol{y}_{\mathrm{q}}[k] = \boldsymbol{y}[k]+\boldsymbol{v}_{\mathrm{q}}[k]$, i.e.,

$$\boldsymbol{y}_{\mathrm{q}}[k] = \boldsymbol{C}\boldsymbol{x}[k] + \boldsymbol{v}_{\mathrm{q}}[k], \tag{2}$$

where $\boldsymbol{v}_{\mathrm{q}}[k] \in \mathbb{R}^{N_{\mathrm{y}}}$ is a quantization noise vector that is modeled as a uniform random vector whose mean vector and covariance matrix are $\boldsymbol{0}$ and $\boldsymbol{V}_{\mathrm{q}}$, respectively. $\boldsymbol{V}_{\mathrm{q}}$ is given as a diagonal matrix whose i-th ($i = 0, 1, \ldots, N_{\mathrm{y}}-1$) diagonal element is $V_{\mathrm{q}\,i} = \Delta_i^2/12$, where Δ_i is the value of the resolution of the quantization for each element of $\boldsymbol{y}_{\mathrm{q}}[k]$.

3) State observer: At each time index, the state observer receives $\hat{\boldsymbol{y}}_{\mathrm{q}}[k] \in \mathbb{R}^{N_{\mathrm{y}}}$, which is a decoded version of $\boldsymbol{y}_{\mathrm{q}}[k]$, including undetected bit errors, and an error detection result from the communication layer, i.e., the receiver. Using them, the state observer calculates the estimated state vector $\tilde{\boldsymbol{x}}[k+1] \in \mathbb{R}^{N_{\mathrm{y}}}$, which corresponds to the unknown $\boldsymbol{x}[k+1]$ of the next time index, according to the control system equations in (1) and (2). According to [5], a Kalman filter-based state observer is employed, and the calculation steps are described as follows.

⟨1. Gain calculation step⟩

$$\boldsymbol{K}_{\mathrm{o}}[k] = \boldsymbol{\Pi}[k]\boldsymbol{C}^{\mathrm{T}}(\boldsymbol{C}\boldsymbol{\Pi}[k]\boldsymbol{C}^{\mathrm{T}} + \boldsymbol{V}[k])^{-1} \tag{3}$$

⟨2. Update step⟩

If no bit error is detected,

$$\tilde{\boldsymbol{x}}_{+}[k] = \tilde{\boldsymbol{x}}[k] + \boldsymbol{K}_{\mathrm{o}}[k](\hat{\boldsymbol{y}}_{\mathrm{q}}[k] - \tilde{\boldsymbol{y}}[k]), \tag{4}$$

$$\boldsymbol{\Pi}_{+}[k] = (\boldsymbol{I} - \boldsymbol{K}_{\mathrm{o}}[k]\boldsymbol{C})\boldsymbol{\Pi}[k]. \tag{5}$$

Otherwise,

$$\tilde{\boldsymbol{x}}_{+}[k] = \tilde{\boldsymbol{x}}[k], \tag{6}$$

$$\boldsymbol{\Pi}_{+}[k] = \boldsymbol{\Pi}[k]. \tag{7}$$

⟨3. Prediction step⟩

$$\tilde{\boldsymbol{x}}[k+1] = \boldsymbol{A}\tilde{\boldsymbol{x}}_{+}[k] + \boldsymbol{B}\boldsymbol{u}_{\mathrm{q}}[k] \tag{8}$$

$$\boldsymbol{\Pi}[k+1] = \boldsymbol{A}\boldsymbol{\Pi}_{+}[k]\boldsymbol{A}^{\mathrm{T}} + \boldsymbol{W} \tag{9}$$

In (3)–(9), $\tilde{\boldsymbol{y}}[k]$ is defined as $\tilde{\boldsymbol{y}}[k] = \boldsymbol{C}\tilde{\boldsymbol{x}}[k]$ and represents an estimated version of $\boldsymbol{y}[k]$, and $\boldsymbol{I}$ is an identity matrix with the appropriate dimension. In the calculation steps, $\boldsymbol{K}_{\mathrm{o}}[k] \in \mathbb{R}^{N_{\mathrm{x}}\times N_{\mathrm{y}}}$ is calculated as an observer gain matrix, and $\boldsymbol{\Pi}[k] \in \mathbb{R}^{N_{\mathrm{x}}\times N_{\mathrm{x}}}$ is calculated as the covariance matrix

of the estimation error vector $\boldsymbol{e}[k]\,(=\boldsymbol{x}[k]-\tilde{\boldsymbol{x}}[k])$. $\boldsymbol{V}[k]\in\mathbb{R}^{N_\mathrm{y}\times N_\mathrm{y}}$ is the covariance matrix of $\boldsymbol{y}[k]-\hat{\boldsymbol{y}}_\mathrm{q}[k]$. For the above calculation, $\boldsymbol{A}$, $\boldsymbol{B}$, $\boldsymbol{C}$, and $\boldsymbol{W}$ are assumed to be known at the state observer.

In this paper, in contrast to [5], $\boldsymbol{V}[k]$ is given as $\boldsymbol{V}[k]=\boldsymbol{V}_\mathrm{q}+\boldsymbol{V}_\mathrm{ud}[k]$, where $\boldsymbol{V}_\mathrm{ud}[k]\in\mathbb{R}^{N_\mathrm{y}\times N_\mathrm{y}}$ is the covariance matrix of the effect of undetected bit errors on $\hat{\boldsymbol{y}}_\mathrm{q}[k]$ and added to reduce the effect of undetected bit errors. This equation is based on the fact that the effect of quantization noise and that of channel bit errors can be separately described in the case of uniform quantization and natural binary index assignment (and also Gray code) [27]. The calculation of $\boldsymbol{V}_\mathrm{ud}[k]$ is explained in detail in Section III.

4) Controller: Using the reference state vector $\boldsymbol{x}_\mathrm{ref}[k]\in\mathbb{R}^{N_\mathrm{x}}$ and the estimated state vector $\tilde{\boldsymbol{x}}[k]$ of the state observer, the controller calculates the input vector $\boldsymbol{u}[k]\in\mathbb{R}^{N_\mathrm{u}}$ as

$$\boldsymbol{u}[k]=\boldsymbol{K}_\mathrm{c}(\boldsymbol{x}_\mathrm{ref}[k]-\tilde{\boldsymbol{x}}[k]), \tag{10}$$

where $\boldsymbol{K}_\mathrm{c}\in\mathbb{R}^{N_\mathrm{u}\times N_\mathrm{x}}$ is the controller gain matrix. Then, $\boldsymbol{u}[k]$ is transformed into $\boldsymbol{u}_\mathrm{q}[k]$ via the analog-to-digital conversion and input into the plant. L-bit mid-tread uniform quantization is used for this conversion, and each vector element of $\boldsymbol{u}_\mathrm{q}[k]$ is quantized as an L-bit digital value; to simplify the notation, the same bit length is used for all vector elements.

B. Communication layer

The transmitter encodes the observed state ($\boldsymbol{y}_\mathrm{q}[k]$) with an error detection code and transmits the encoded bits as a modulated signal ($\boldsymbol{s}[k]$) to the receiver via a noisy channel. The transmitted signal is affected by fading ($\boldsymbol{H}[k]$) and channel noise ($\boldsymbol{n}[k]$). The receiver determines the most probable state as the received state ($\hat{\boldsymbol{y}}_\mathrm{q}[k]$) from the demodulated signal ($\boldsymbol{r}[k]$). Even if there is only a one-bit error, it may cause the received state to jump to a very different state from the true state; therefore, error detection is performed to discard the erroneous received state.

Note that all of the signal representations ($\boldsymbol{s}[k]$, $\boldsymbol{r}[k]$, $\boldsymbol{n}[k]$, and $\boldsymbol{H}[k]$) in the communication layer are defined as vectors or matrices in an arbitrary real or complex signal space such as the two-dimensional signal space of phase shift keying and quadrature amplitude modulation.

1) Transmitter: At each time index, $\boldsymbol{y}_\mathrm{q}[k]$ is mapped to natural binary indices and interpreted as a data bit sequence of $N_\mathrm{y}L$ bits. The natural binary index assignment is very simple but one of the best index assignments for uniform quantization, which minimizes the mean squared error distortion in the quantized values resulting from channel bit errors [27]. Then, to detect

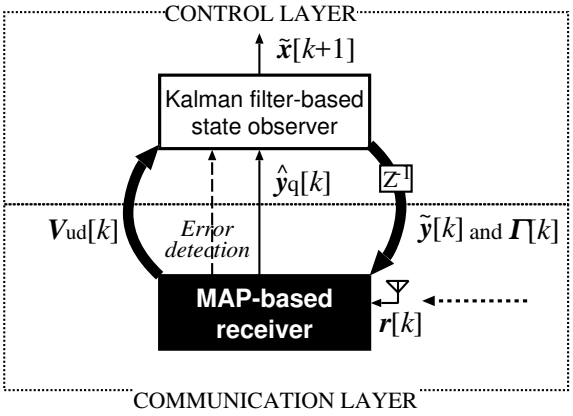

Fig. 2. Structure of our cross-layer optimized receiver.

the bit errors at the receiver, the $N_{\mathrm{y}}L$-bit data sequence is encoded by an error detection code, namely, a cyclic redundancy code (CRC) with M-bit parity; therefore, the total bit length of the transmitted data packet corresponding to $\boldsymbol{y}_{\mathrm{q}}[k]$ is $N_{\mathrm{y}}L + M$.

The encoded sequence is modulated to a digital signal and transmitted to the receiver. The transmitted signal is represented as the signal vector $\boldsymbol{s}[k]$ in a signal space representation, and the transmitted signal energy per data bit is E_{b}.

2) Channel: The transmission of $\boldsymbol{s}[k]$ from the transmitter to the receiver is assumed to be completed within one control loop of T_{s}. The channel from the transmitter to the receiver is assumed to be memoryless and a fading channel with additive white Gaussian noise, where the demodulated signal is represented as the signal vector $\boldsymbol{r}[k] = \boldsymbol{H}[k]\boldsymbol{s}[k]+\boldsymbol{n}[k]$. $\boldsymbol{H}[k]$ is a channel matrix that represents the fading coefficients. $\boldsymbol{n}[k]$ is a white Gaussian random vector in which the power spectrum density of each vector element is $N_0/2$. The SNR per data bit is defined as E_{b}/N_0. $\boldsymbol{H}[k]$ is assumed to be known at the receiver.

3) Receiver: According to optimal decision theory, the receiver first determines the most probable transmitted bit sequence from $\boldsymbol{r}[k]$, and the leading $N_{\mathrm{y}}L$ bits are demapped to $\hat{\boldsymbol{y}}_{\mathrm{q}}[k]$. The proposed receiver design is explained in detail in Section III. Next, error detection is performed using the determined bit sequence. If no bit error is detected, $\hat{\boldsymbol{y}}_{\mathrm{q}}[k]$ is input into the control layer, i.e., the state observer; otherwise, $\hat{\boldsymbol{y}}_{\mathrm{q}}[k]$ is discarded.

III. Proposed Receiver Design

The structure of our cross-layer optimized receiver is shown in Figure 2. The proposed receiver is a MAP-based receiver connected with the Kalman filter-based state observer by a recursive structure over the control layer and communication layer. It utilizes the estimated vector $\tilde{\boldsymbol{y}}[k]$ and covariance matrix $\boldsymbol{\Gamma}[k]$ of the state observer as the à priori information and minimizes the channel error probability of $\hat{\boldsymbol{y}}_{\mathrm{q}}[k]$ on the basis of the MAP decision. The details of the MAP receiver are explained in Section III-A. In addition, the proposed receiver provides the covariance matrix $\boldsymbol{V}_{\mathrm{ud}}[k]$ of the effect of undetected bit errors on $\hat{\boldsymbol{y}}_{\mathrm{q}}[k]$ for the state observer. The details of the covariance matrix are explained in Section III-B.

A. MAP receiver with the estimated state information of the state observer

Each element $\hat{y}_{\mathrm{q}\,i}[k]$ of $\hat{\boldsymbol{y}}_{\mathrm{q}}[k]$ is encoded with L bits; therefore, the MAP decision of $\hat{y}_{\mathrm{q}\,i}[k]$ refers to the decision of a 2^L-ary symbol.

First, we present a brief description of the maximum likelihood (ML) receiver, which is the optimal receiver for minimizing the channel error in the case with no à priori information, i.e., the probability density (or mass) function, of the transmitted output vector. The ML receiver determines $\hat{y}_{\mathrm{q}\,i}[k]$ to minimize the channel error probability $\mathrm{P}(\hat{y}_{\mathrm{q}\,i}[k] \neq y_{\mathrm{q}\,i}[k])$ according to the following criterion.

$$\hat{y}_{\mathrm{q}\,i}[k] = \underset{y_{\mathrm{q}\,i}[k]}{\arg\max}\, \mathrm{P}(\boldsymbol{r}_i[k] \mid y_{\mathrm{q}\,i}[k]) = \underset{y_{\mathrm{q}\,i}[k](\equiv \boldsymbol{s}_i[k])}{\arg\max} \left\{ -\frac{1}{N_0} ||\boldsymbol{r}_i[k] - \boldsymbol{H}_i[k]\boldsymbol{s}_i[k]||^2 \right\}, \tag{11}$$

where "≡" denotes equivalent information resulting from the one-to-one mapping. $\boldsymbol{r}_i[k]$, $\boldsymbol{s}_i[k]$, and $\boldsymbol{H}_i[k]$ denote the subvectors of $\boldsymbol{r}[k]$ and $\boldsymbol{s}[k]$ and the submatrix of $\boldsymbol{H}[k]$, respectively, which correspond to each element $y_{\mathrm{q}\,i}[k]$ of $\boldsymbol{y}_{\mathrm{q}}[k]$.

In contrast to the ML receiver, the proposed receiver is a MAP receiver, which is the optimal receiver for minimizing the channel error in the case with the à priori information of the transmitted output vector. The proposed MAP receiver utilizes the previously calculated $\tilde{\boldsymbol{y}}[k]$ of the state observer as the à priori information of the transmitted output vector. It is formulated as a MAP decision with the conditional à priori probability $\mathrm{P}(y_{\mathrm{q}\,i}[k] \mid \tilde{y}_i[k])$ corresponding to each element $\tilde{y}_i[k]$ of $\tilde{\boldsymbol{y}}[k]$. To minimize $\mathrm{P}(\hat{y}_{\mathrm{q}\,i}[k] \neq y_{\mathrm{q}\,i}[k])$, the proposed MAP receiver determines $\hat{y}_{\mathrm{q}\,i}[k]$ according to the following criterion:

$$\hat{y}_{\mathrm{q}\,i}[k] = \underset{y_{\mathrm{q}\,i}[k]}{\arg\max}\, \mathrm{P}(\boldsymbol{r}_i[k] \mid y_{\mathrm{q}\,i}[k])\ \mathrm{P}(y_{\mathrm{q}\,i}[k] \mid \tilde{y}_i[k]). \tag{12}$$

$\mathrm{P}(y_{\mathrm{q}i}[k] \mid \tilde{y}_i[k])$ is obtained from the state observer as follows. The relationship between $\boldsymbol{y}_{\mathrm{q}}[k]$ and $\tilde{\boldsymbol{y}}[k]$ is formulated as

$$\begin{aligned}\boldsymbol{y}_{\mathrm{q}}[k] &= \boldsymbol{y}[k] + \boldsymbol{v}_{\mathrm{q}}[k] \\ &= \tilde{\boldsymbol{y}}[k] + \boldsymbol{C}\boldsymbol{e}[k] + \boldsymbol{v}_{\mathrm{q}}[k] \quad (\because \boldsymbol{e}[k] = \boldsymbol{x}[k] - \tilde{\boldsymbol{x}}[k]) \\ &= \tilde{\boldsymbol{y}}[k] + \boldsymbol{\gamma}[k], \end{aligned} \tag{13}$$

where $\boldsymbol{\gamma}[k]$ is defined as $\boldsymbol{\gamma}[k] = \boldsymbol{C}\boldsymbol{e}[k] + \boldsymbol{v}_{\mathrm{q}}[k]$ and represents the difference between $\boldsymbol{y}_{\mathrm{q}}[k]$ and $\tilde{\boldsymbol{y}}[k]$. The mean vector of $\boldsymbol{\gamma}[k]$ is $\boldsymbol{0}$. Here, $\boldsymbol{C}\boldsymbol{e}[k]$ and $\boldsymbol{v}_{\mathrm{q}}[k]$ are not necessarily independent. If they are independent, the covariance matrix of $\boldsymbol{\gamma}[k]$ is given by the sum of the covariance matrices of each term, i.e., $\boldsymbol{C}\boldsymbol{\Pi}[k]\boldsymbol{C}^{\mathrm{T}} + \boldsymbol{V}_{\mathrm{q}}$; otherwise, it is given as $\boldsymbol{C}\boldsymbol{\Pi}[k]\boldsymbol{C}^{\mathrm{T}} + \boldsymbol{V}_{\mathrm{q}} + \mathrm{COV}\{\boldsymbol{C}\boldsymbol{e}[k], \boldsymbol{v}_{\mathrm{q}}[k]\} + \mathrm{COV}\{\boldsymbol{C}\boldsymbol{e}[k], \boldsymbol{v}_{\mathrm{q}}[k]\}^{\mathrm{T}}$, where $\mathrm{COV}\{\boldsymbol{C}\boldsymbol{e}[k], \boldsymbol{v}_{\mathrm{q}}[k]\}$ is the cross-covariance between the vectors $\boldsymbol{C}\boldsymbol{e}[k]$ and $\boldsymbol{v}_{\mathrm{q}}[k]$. Because it is both theoretically and experimentally difficult to obtain the cross-covariance term, it is ignored for ease of computation in the same way as the Kalman filer-based state observer. With this approximation, the covariance matrix of $\boldsymbol{\gamma}[k]$ is given as $\boldsymbol{C}\boldsymbol{\Pi}[k]\boldsymbol{C}^{\mathrm{T}} + \boldsymbol{V}_{\mathrm{q}}$ and available from (3) for the state observer; therefore, no additional calculation is required to obtain the covariance matrix. For convenience, $\boldsymbol{\Gamma}[k]$ is defined as $\boldsymbol{\Gamma}[k] = \boldsymbol{C}\boldsymbol{\Pi}[k]\boldsymbol{C}^{\mathrm{T}} + \boldsymbol{V}_{\mathrm{q}}$. Then, roughly approximating $\boldsymbol{\gamma}[k]$ as Gaussian for ease of computation, $\mathrm{P}(y_{\mathrm{q}i}[k] \mid \tilde{y}_i[k])$ is given as

$$\mathrm{P}(y_{\mathrm{q}i}[k] \mid \tilde{y}_i[k]) \approx \frac{1}{\sqrt{2\pi\Gamma_i[k]}} \exp\left(-\frac{1}{2\Gamma_i[k]}(y_{\mathrm{q}i}[k] - \tilde{y}_i[k])^2\right), \tag{14}$$

where $\Gamma_i[k]$ denotes the i-th diagonal element of $\boldsymbol{\Gamma}[k]$.

Finally, substituting (14) into (12), the MAP decision is simplified as

$$\hat{y}_{\mathrm{q}i}[k] = \underset{y_{\mathrm{q}i}[k](\equiv \boldsymbol{s}_i[k])}{\arg\max} \left\{ -\frac{1}{N_0}||\boldsymbol{r}_i[k] - \boldsymbol{H}_i[k]\boldsymbol{s}_i[k]||^2 - \frac{1}{2\Gamma_i[k]}(y_{\mathrm{q}i}[k] - \tilde{y}_i[k])^2 \right\}. \tag{15}$$

Thus, the proposed MAP receiver determines $\hat{\boldsymbol{y}}_{\mathrm{q}}[k]$ by utilizing $\tilde{\boldsymbol{y}}[k]$ and $\boldsymbol{\Gamma}[k]$, which were previously calculated in the state observer, and can be simply implemented. The computational difference between (11) of the ML receiver and (15) of the proposed MAP receiver appears only in the second term, which is the term representing the à priori information. The second term has only one subtraction, one division, and one squaring process, and its necessary variables $\tilde{y}_i[k]$ and $\Gamma_i[k]$ are directly obtained from the state observer without additional computation; therefore, compared with (11) of the ML receiver, (15) of the proposed MAP receiver does not have much complexity for digital computation.

Note that the received parity bits are determined according to the ML decision because the parity bits depend on all of the elements of the transmitted vector $\boldsymbol{y}_{\mathrm{q}}[k]$, and it is complex to calculate the à priori information of the parity bits.

B. Covariance matrix of the effect of undetected bit errors for the state observer

Even if no bit error is detected by error detection after the MAP decision, undetected bit errors may be included in the determined bit sequence with a probability $P_{\mathrm{ud}}[k]$. This is not negligible at a low SNR and leads to deterioration in the control performance; therefore, to reduce the effect of undetected bit errors on $\hat{\boldsymbol{y}}_{\mathrm{q}}[k]$, the receiver should provide an appropriate covariance matrix of $\boldsymbol{y}_{\mathrm{q}}[k] - \hat{\boldsymbol{y}}_{\mathrm{q}}[k]$, i.e., $\boldsymbol{V}_{\mathrm{ud}}[k]$, to the state observer.

Because the undetected error patterns of the error detection code do not depend on the elements of $\boldsymbol{y}_{\mathrm{q}}[k]$, $\boldsymbol{V}_{\mathrm{ud}}[k]$ can be treated as a diagonal matrix; therefore, we only have to consider the i-th diagonal element of $\boldsymbol{V}_{\mathrm{ud}}[k]$, i.e., the variance of $y_{\mathrm{q}\,i}[k] - \hat{y}_{\mathrm{q}\,i}[k]$.

Before error detection, the variance of $y_{\mathrm{q}\,i}[k] - \hat{y}_{\mathrm{q}\,i}[k]$ is given as follows [27]:

$$\mathrm{VAR}\left\{y_{\mathrm{q}\,i}[k] - \hat{y}_{\mathrm{q}\,i}[k]\right\} = \sum_{\ell=0}^{L-1} (2^{\ell} \Delta_i)^2 p_{\ell+iL}[k], \tag{16}$$

where $p_{\ell+iL}[k]$ is the bit error rate (BER) at the ℓ-th bit of $\hat{y}_{\mathrm{q}\,i}[k]$. This equation is derived from all possible errors in each bit of $\hat{y}_{\mathrm{q}\,i}[k]$. After error detection, the determined bit sequence that has detectable error patterns is discarded and not used in the state observer; thus, $\hat{y}_{\mathrm{q}\,i}[k]$ includes only undetected bit errors. Therefore, instead of (16), the i-th diagonal element of $\boldsymbol{V}_{\mathrm{ud}}[k]$ should be

$$V_{\mathrm{ud}\,i} = \sum_{\ell=0}^{L-1} (2^{\ell} \Delta_i)^2 \,\mathrm{P}\left(\begin{array}{l|l} \text{An undetected error occurs} & \text{No bit error is detected} \\ \text{in the } \ell\text{-th bit of } \hat{y}_{\mathrm{q}\,i}[k] & \text{in the determined bit sequence} \end{array} \right). \tag{17}$$

However, it is difficult to directly derive (17) because the undetected bit errors are related to L bits and all $N_{\mathrm{y}}L + M$ bits of the determined bit sequence. To calculate $V_{\mathrm{ud}\,i}[k]$, we write the following simple approximation:

$$\begin{aligned} V_{\mathrm{ud}\,i} &\approx \sum_{\ell=0}^{L-1} (2^{\ell} \Delta_i)^2 p_{\ell+iL}[k] \,\mathrm{P}\left(\begin{array}{l|l} \text{Undetected errors occur} & \text{No bit error is detected} \\ \text{in the determined bit sequence} & \text{in the determined bit sequence} \end{array} \right) \\ &= \sum_{\ell=0}^{L-1} (2^{\ell} \Delta_i)^2 p_{\ell+iL}[k] \frac{P_{\mathrm{ud}}[k]}{(1 - P_{\mathrm{e}}[k]) + P_{\mathrm{ud}}[k]}, \end{aligned} \tag{18}$$

where $P_{\mathrm{e}}[k]$ is the packet error rate (PER), i.e., the probability that bit errors occur in the determined bit sequence; and $P_{\mathrm{ud}}[k]$ is the probability that undetected bit errors occur in the

determined bit sequence. The denominator, $(1 - P_{\mathrm{e}}[k]) + P_{\mathrm{ud}}[k]$, is the probability that no bit error is detected by error detection. Here, the PER is given as

$$P_{\mathrm{e}}[k] = 1 - \sum_{n=0}^{N_{\mathrm{y}}L+M-1} (1 - p_n[k]). \tag{19}$$

The undetected error probability is upper-bounded by a function of the worst BER $p_{n'}[k] (= \max_{n=0}^{N_{\mathrm{y}}L+M-1} p_n[k])$ as follows:

$$P_{\mathrm{ud}}[k] \leq \sum_{d=d_{\min}}^{N_{\mathrm{y}}L+M} \alpha_d \, p_{n'}[k]^d (1 - p_{n'}[k])^{N_{\mathrm{y}}L+M-d}, \tag{20}$$

where $d_{\min}$ and α_d are the minimum distance and weight distribution of the CRC.

To summarize (18)–(20), $\boldsymbol{V}_{\mathrm{ud}}[k]$ is calculated as a function of $\{p_n[k] \mid n = 0, 1, \ldots, N_{\mathrm{y}}L + M - 1\}$. At the proposed receiver, $p_n[k]$ can be estimated by the well-known approaches of MAP decoding. According to [28], $p_n[k]$ is estimated by using the log likelihood rate (LLR) $\mathrm{LLR}_n[k]$ of each determined bit as follows:

$$p_n[k] \approx \frac{1}{1 + \exp |\mathrm{LLR}_n[k]|}. \tag{21}$$

$\mathrm{LLR}_n[k]$ can be converted from the maximizing term in (15) in the same way as (6) of [29], which is merely a log-sum-exp computation. In detail, the LLR of the ℓ-th bit of $\hat{y}_{\mathrm{q}i}[k]$ is calculated as

$$\mathrm{LLR}_{\ell+iL}[k] \approx \max_{y_{\mathrm{q}i}[k]\colon \text{ the } \ell\text{-th bit is } 1} f(y_{\mathrm{q}i}[k]) - \max_{y_{\mathrm{q}i}[k]\colon \text{ the } \ell\text{-th bit is } 0} f(y_{\mathrm{q}i}[k]), \tag{22}$$

where $f(y_{\mathrm{q}i}[k])$ is the maximizing term in (15). The first term in (22) represents the maximum value of $f(y_{\mathrm{q}i}[k])$ only for $y_{\mathrm{q}i}[k]$ whose ℓ-th bit is 1, and the second term is that for $y_{\mathrm{q}i}[k]$ whose ℓ-th bit is 0. These terms can be calculated with a small cost at the same time during the calculation of (15). The above calculation is applicable to the proposed and ML receivers with the maximizing term in (11) instead of (15).

IV. Numerical Results

A. Simulation setup

Computer simulations were performed to evaluate the performance of the proposed scheme. A rotary inverted pendulum (Furuta pendulum) was employed as an example of the plant. It is a typical under-actuated object and widely used as a control performance measure. Figure 3 shows the basic structure of the rotary inverted pendulum. Table I summarizes the parameters

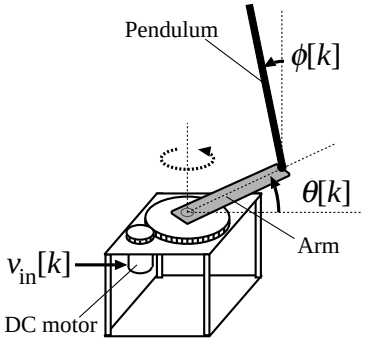

Fig. 3. Rotary inverted pendulum.

TABLE I

ROTARY INVERTED PENDULUM PARAMETERS.

Mass of the pendulum	0.016 (kg)
Length of the pendulum	0.20 (m)
Length of the arm	0.20 (m)
Central Moment of inertia of the arm	0.0048 (kgm^2)
DC motor's resistance	8.3 (Ω)
DC motor's torque constant	0.023 (Nm/A,Vs/rad)
Gear ratio (Arm / DC motor)	120/16
Gravitational constant	9.81 (m/s^2)

based on RealTEC RTC05 [30]. The sampling interval is set to $T_{\mathrm{s}} = 0.01$ s, and $\boldsymbol{A}$ and $\boldsymbol{B}$ of the discretized system are given as follows:

$$\boldsymbol{A} = \begin{bmatrix} 1.006 & 0 & 1.002 \times 10^{-2} & 7.457 \times 10^{-5} \\ -3.265 \times 10^{-4} & 1 & -1.089 \times 10^{-6} & 9.963 \times 10^{-3} \\ 1.113 & 0 & 1.006 & 1.491 \times 10^{-2} \\ -6.528 \times 10^{-2} & 0 & -3.265 \times 10^{-4} & 9.926 \times 10^{-1} \end{bmatrix}, \quad \boldsymbol{B} = \begin{bmatrix} -4.323 \times 10^{-4} \\ 2.160 \times 10^{-4} \\ -8.643 \times 10^{-2} \\ 4.315 \times 10^{-2} \end{bmatrix}. \tag{23}$$

In this plant, $\boldsymbol{u}[k]$ is the one-dimensional vector $\boldsymbol{u}[k] = [u_{\mathrm{in}}[k]]$ ($N_{\mathrm{u}} = 1$), where $u_{\mathrm{in}}[k]$ denotes the input voltage to the direct current (DC) motor. $\boldsymbol{x}[k]$ is the four-dimensional vector $\boldsymbol{x}[k] = [\phi[k] \quad \theta[k] \quad \dot{\phi}[k] \quad \dot{\theta}[k]]^{\mathrm{T}}$ ($N_{\mathrm{x}} = 4$), where $\phi[k]$ and $\dot{\phi}[k]$ are the angle and angular velocities of the pendulum, respectively. $\theta[k]$ and $\dot{\theta}[k]$ are the angle and angular velocities of the arm, respectively. The angles are observed by sensors, but the angular velocities are not, i.e.,

$N_\mathrm{y} = 2$. Further, the output matrix is written as

$$\boldsymbol{C} = \begin{bmatrix} 1 & 0 & 0 & 0 \\ 0 & 1 & 0 & 0 \end{bmatrix}. \tag{24}$$

A linear quadratic Gaussian controller is employed as the controller. It has been widely studied in the field of networked control and shown to be an asymptotically stable controller over communication channels with channel errors. According to [5], $\boldsymbol{K}_\mathrm{c}$ is calculated as the gain matrix that minimizes the expectation of the following quadratic cost:

$$\lim_{K\to\infty} \frac{1}{K} \sum_{k=0}^{K} \left(\boldsymbol{x}[k]^\mathrm{T} \boldsymbol{Q}_\mathrm{x} \boldsymbol{x}[k] + \boldsymbol{u}[k]^\mathrm{T} \boldsymbol{Q}_\mathrm{u} \boldsymbol{u}[k] \right), \tag{25}$$

where $\boldsymbol{Q}_\mathrm{x}$ and $\boldsymbol{Q}_\mathrm{u}$ are the arbitrary weight matrices for the state and input vectors. To limit $|u_\mathrm{in}[k]| \leq 8.0$, the weight matrices are adequately set to $\boldsymbol{Q}_\mathrm{x} = \boldsymbol{C}^\mathrm{T}\boldsymbol{C}$ and $\boldsymbol{Q}_\mathrm{u} = [0.24]$. Note that the proposed receiver depends on the functional relations of the state observer but not on those of the controller and thus can be applied with other types of controllers such as H_∞ and model predictive controllers.

For simplicity, $\boldsymbol{W}$ is set to a diagonal matrix whose diagonal elements are all equal to σ_w^2, where σ_w is used as a variable for performance evaluation. For quantization, the resolution of the L-bit uniform quantization is set to $8.0/2^{L-1}$ V for $\boldsymbol{u}_\mathrm{q}[k]$ and $\Delta_1 = \Delta_2 = \pi/2^{L-1}$ rad for $\boldsymbol{y}_\mathrm{q}[k]$. L is used as a variable for the performance evaluation and set to $L = 8, 10, 12$, and 16, which are reasonable values for realistic analog-to-digital conversion.

The control objective of the rotary inverted pendulum is to enable the arm angle $\theta[k]$ to follow the target value $\Theta[k]$ while maintaining the pendulum's upright position, i.e., $\boldsymbol{x}_\mathrm{ref}[k] = [0 \;\; \Theta[k] \;\; 0 \;\; 0]^\mathrm{T}$. Here, $\Theta[k]$ is set to a rectangular signal alternately switching between $\pi/2$ rad and $-\pi/2$ rad every 10 s. $\boldsymbol{x}[0] = \tilde{\boldsymbol{x}}[0] = \boldsymbol{0}$ and $\boldsymbol{\Pi}[0] = \boldsymbol{0}$ are set as the initial values. The simulation time is 1000 s, and the number of simulation runs is 10^4. Here, once $|\phi[k]| > \pi/2$, it is assumed that the pendulum has fallen. Once the pendulum falls, the simulation run is terminated.

We focus on wireless networked control in indoor environments such as factory buildings, and a Rayleigh fading channel is selected as the channel model for the channel from the transmitter to the receiver. It is a well-known fading channel model and used as a benchmark for evaluating the performance. In fact, as revealed in some studies, e.g., [31], [32], fading is slow and Rayleigh in heavily cluttered line-of-sight and lightly cluttered obstructed topographies in factory buildings.

The channel is assumed to be independent of other packet transmission and static within one packet transmission, and binary phase shift keying is employed for signal modulation. Thus, the channel matrix is defined as a real diagonal matrix that has the same single Rayleigh distributed random value at all diagonal positions. As explained in Section II-B, an M-bit CRC is added to each data sequence that has $N_{\mathrm{y}}L$ bits corresponding to $\boldsymbol{y}_{\mathrm{q}}[k]$, i.e., the bit length of each transmitted data packet is $N_{\mathrm{y}}L + M$. M is used as a variable for the performance evaluation but should be selected to match the transmitted data length. The best CRCs for $M = 10, 12, 16$, and 20, which respectively have the polynomials 0x2b9, 0xb41, 0x9eb2, and 0xbe73e in implicit +1 octal notation, are selected according to [33].

In Sections IV-B–IV-D, we compare the performance of the proposed receiver and that of the ML receiver. The performance of the communication layer is evaluated by the PERs at the proposed and ML receivers. The performance of the control layer is evaluated by the root mean square error (RMSE) of the arm angle against the ideal control case without system disturbances, quantization, and channel errors. The control performance is highly affected by system disturbances, quantization, and channel errors. To evaluate various cases, simulations have been conducted for different values of σ_{w}, L, E_{b}/N_0, and M.

The ML receiver is the optimal decision for minimizing the channel error in the case with no a priori information, and the proposed receiver is the optimal decision in the case where a priori information is obtained from the state observer in the control layer. To evaluate the effectiveness of the proposed receiver, a comparison with the ML receiver is the fairest. As explained in Section III-A, the proposed receiver operates according to (15), and the ML receiver operates according to (11). Note that in the case without $\boldsymbol{V}_{\mathrm{ud}}$ at the state observer, i.e., with $\boldsymbol{V}_{\mathrm{ud}} = \boldsymbol{0}$, all of the simulations in the given SNR range result in falling of the pendulum. This is because the state observer cannot reduce the effect of undetected bit errors in received state feedback at all. Therefore, the comparison between the proposed receiver with $\boldsymbol{V}_{\mathrm{ud}}$ and the ML receiver without $\boldsymbol{V}_{\mathrm{ud}}$ is not fair. In the following performance comparison, we evaluated the case in which both the proposed and ML receivers provide $\boldsymbol{V}_{\mathrm{ud}}$ for the state observer. As explained in Section III-B, the proposed receiver calculates $\boldsymbol{V}_{\mathrm{ud}}$ according to (18)–(22). The ML receiver also calculates $\boldsymbol{V}_{\mathrm{ud}}$ according to (18)–(22), but (22) is calculated using the maximizing term in (11) instead of (15) of the proposed receiver.

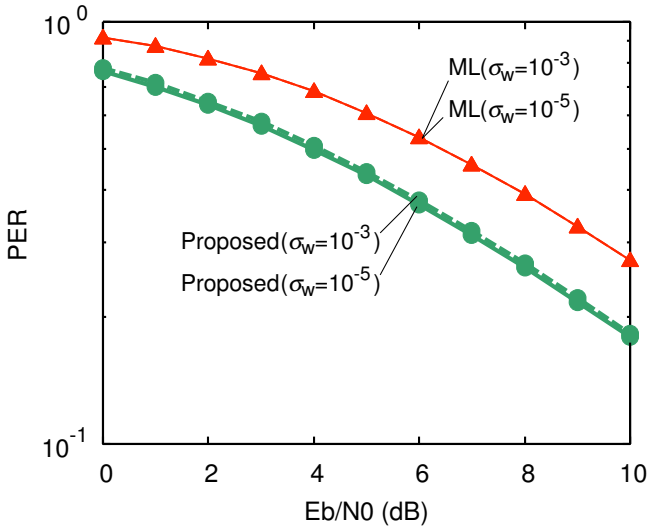

Fig. 4. PER performance versus E_b/N_0 in the presence of different system disturbances.

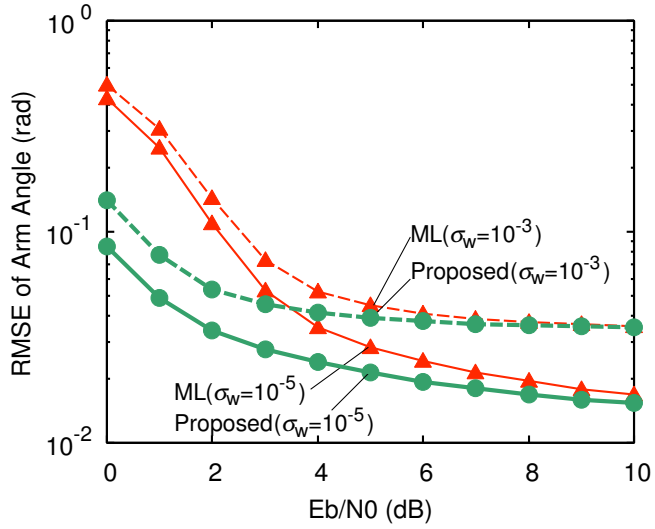

Fig. 5. RMSE performance versus E_b/N_0 in the presence of different system disturbances.

B. Comparison in the presence of different system disturbances

First, the performance is evaluated in the presence of a smaller system disturbance, $\sigma_w = 10^{-5}$, and a larger system disturbance, $\sigma_w = 10^{-3}$. Figures 4 and 5 show the PER and RMSE performance versus E_b/N_0, respectively. Here, $L = 10$. In Figures 4 and 5, the performance of the proposed MAP receiver, denoted as "Proposed," is compared with that of the ML receiver, denoted as "ML".

From Figure 4, we can see that the proposed receiver outperforms the ML receiver and results

in a PER that is ∼1.5 times smaller, i.e., a BER that is ∼20 times smaller. The ML receiver does not depend on the control layer's information; therefore, the PER performance of the ML receiver for $\sigma_{\mathrm{w}} = 10^{-5}$ and that for $\sigma_{\mathrm{w}} = 10^{-3}$ are the same. On the other hand, the PER performance of the proposed receiver for $\sigma_{\mathrm{w}} = 10^{-5}$ is slightly better than that for $\sigma_{\mathrm{w}} = 10^{-3}$. because the proposed receiver utilizes the estimated state information of the state observer as à priori information to determine the most probable transmitted bit sequence. The second term in (15) of the proposed receiver is the term related to the à priori information and has $\Gamma_i[k]$ in the denominator, which represents the accuracy of the à priori information. For a smaller σ_{w}, $\Gamma_i[k]$ also becomes smaller because of (9) for the state observer, meaning that the accuracy of the à priori information improves. Thus, the second term in (15) becomes more effective for determining the most probable transmitted bit sequence, and improves the PER.

Figure 5 shows that as the system disturbance increases, the RMSE performance of both schemes deteriorates. We can also see that the proposed receiver outperforms the ML receiver and results in a larger improvement in the RMSE, particularly at a lower SNR. As the SNR increases, the influence of channel errors on the control performance decreases significantly; therefore, the performance of the proposed receiver and that of the ML receiver converge at a high SNR.

Note that sudden changes in the plant's state may occur owing to system disturbances; thus, the plant's state possibly jumps to a value that differs from the current prediction only for the most significant bit. In this paper, a Kalman filter, which is a minimum mean square error estimator, is used as the state observer and may not be able to track such sudden changes. Because the proposed receiver depends on the accuracy of the state observer, it cannot improve the performance beyond this accuracy. To provide resilience to such specific events, the accuracy of the state observer should be improved by, e.g., changing the cost function.

C. Comparison at different quantization levels

Next, the performance at different quantization levels, $L = 8, 12$, and 16, is evaluated. Figures 6 and 7 show the PER and RMSE performance versus E_{b}/N_0, respectively. Here, $\sigma_{\mathrm{w}} = 10^{-5}$. As L increases, the quantization error becomes smaller, and the bit length of the transmitted packet becomes longer. Note that E_{b}/N_0 for $L = 8$ is set to be 10/8 times greater than that for $L = 10$, and that for $L = 12$ and 16 is set to be 10/12 and 10/16 times smaller than that for $L = 10$ in order to ensure the same total energy for the transmitted packets.

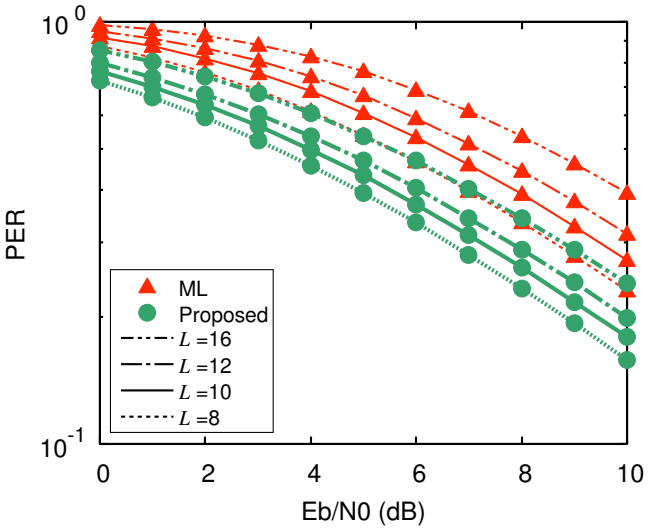

Fig. 6. PER performance versus E_b/N_0 for different quantization levels.

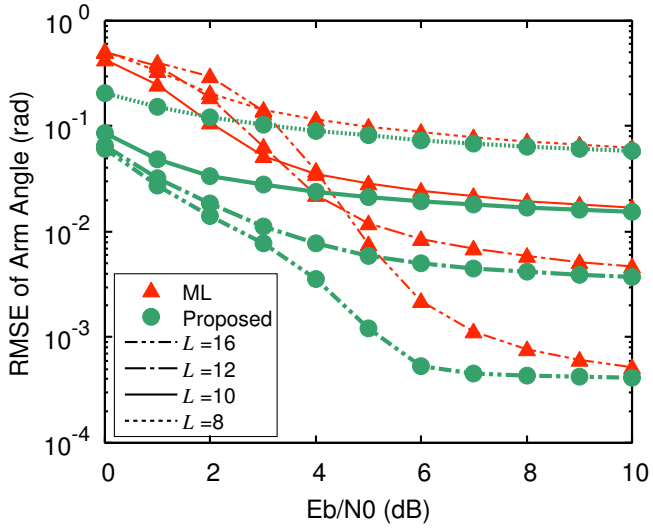

Fig. 7. RMSE performance versus E_b/N_0 for different quantization levels.

As shown in Figure 6, the packet error rate of both the ML and proposed receivers deteriorates as L increases. This is not surprising because of the lower E_b/N_0 for the same total packet energy. Comparing the proposed and ML receivers, we can see that the performance of the proposed receiver is not worse than that of the ML receiver, even at higher values of L. This means that the improvement in the performance obtained by the proposed receiver is larger than the deterioration resulting from a lower E_b/N_0.

The RMSE performance is discussed in two parts: one for a lower L, i.e., $L = 8$, and the

other for a higher L, i.e., L = 12 and 16.

Comparing the cases of L = 8 and L = 10 in Figure 7, we can see that the RMSE performance of both schemes deteriorates. This means that the influence of the quantization error on the control performance is larger than that of the improvement in the PER resulting from a higher E_b/N_0. However, even for a lower L, the proposed receiver can improve both the PER and RMSE performance compared to the ML receiver.

Comparing the cases of L = 12 and 16 with that of L = 10 in Figure 7, we can see that in the case of the ML receiver, as L increases, the RMSE performance improves at a higher SNR and deteriorates at a lower SNR. At a higher SNR, the influence of channel errors on the control performance becomes smaller than that of the quantization error; therefore, the RMSE performance at a higher L, i.e., a smaller quantization error, is better than that at a lower L. At a lower SNR, the influence of channel errors on the control performance becomes larger than that of quantization error; therefore, because of the lower E_b/N_0, the RMSE performance at a higher L, i.e., a higher packet error rate, is worse than that at a lower L. In contrast to the ML receiver, the RMSE performance of the proposed receiver of higher L is better than that of lower L in all SNR regions. As shown in Figure 6, the proposed receiver can reduce the number of channel errors effectively, even at a higher L, and the influence of channel errors on the control performance becomes smaller than that for the ML receiver. Therefore, the RMSE performance at a higher L, i.e., a smaller quantization error, becomes better than that at a lower L.

D. Comparison at different parity bit lengths

Finally, the performance at different parity bit lengths, M = 12, 16, and 20, is evaluated. Figures 8 and 9 show the PER and RMSE performance versus E_b/N_0, respectively. Here, $\sigma_w = 10^{-5}$.

As shown in Figure 8, the PERs of both the ML and proposed receivers deteriorate as M increases. This is not surprising because of the lower signal energy for the same total packet energy. Comparing the proposed and ML receivers, we can see that the proposed receiver can improve the PER, even at a higher M. However, at a higher M, the improvement becomes smaller. This is because the proposed receiver does not reduce the number of channel errors in the parity bits; thus, the channel errors in the parity bits increase the PER of the proposed receiver. This effect remarkably appears at a lower SNR. When M = 20, i.e., half of the length

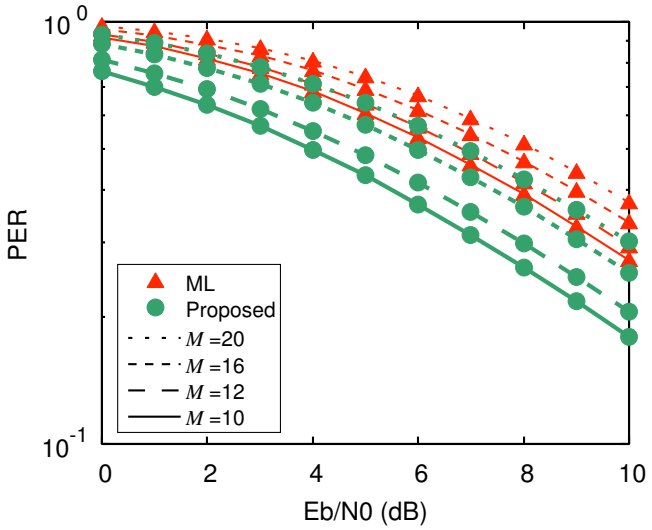

Fig. 8. PER performance versus E_b/N_0 for different parity bit lengths.

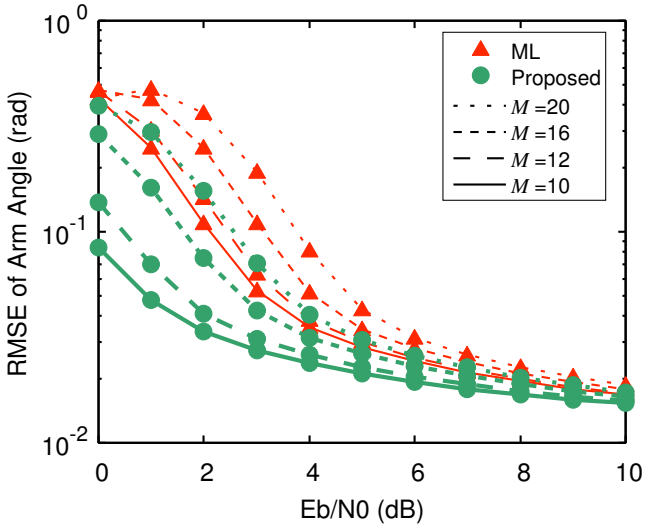

Fig. 9. RMSE performance versus E_b/N_0 for different parity bit lengths.

of the transmitted packet is the parity bits, the PER of the proposed receiver is no longer superior than that of the ML receiver with $M = 10$.

The parity bit length only affects the PER and does not affect the system disturbances and quantization error. Therefore, Figure 9 shows that as M increases, the RMSE performance of both the ML and proposed receivers also deteriorates along with the PER. The proposed receiver can improve the RMSE performance, even at a higher M; however, the effectiveness of the proposed receiver at a lower SNR becomes smaller because of the higher PER.

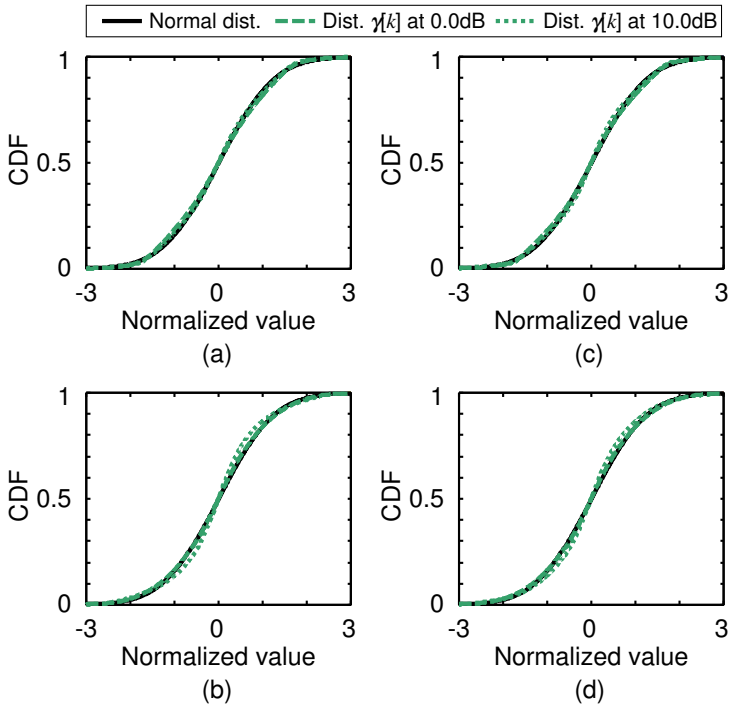

Fig. 10. CDFs of $\boldsymbol{\gamma}[k]$ normalized by $\boldsymbol{\Gamma}[k]$: (a) $L = 10$ & $\sigma_{\mathrm{w}} = 10^{-5}$, (b) $L = 10$ & $\sigma_{\mathrm{w}} = 10^{-3}$, (c) $L = 8$ & $\sigma_{\mathrm{w}} = 10^{-5}$, and (d) $L = 8$ & $\sigma_{\mathrm{w}} = 10^{-3}$.

E. Validity of the approximation for the proposed receiver

To confirm the validity of the Gaussian approximation for $\boldsymbol{\gamma}[k]$ in (14) of the proposed receiver, the cumulative distribution function of $\boldsymbol{\gamma}[k]$ normalized by $\boldsymbol{\Gamma}[k]$ is shown in Figure 10 for some of the parameters used in the above performance evaluation. Here, $M = 10$. In Figure 10, for easy comparison, a one-dimensional CDF is constructed from all of the time samples of all of the normalized elements of $\boldsymbol{\gamma}[k]$. Comparing the CDF of $\boldsymbol{\gamma}[k]$ and that of the normal distribution, we can see that the Gaussian approximation for $\boldsymbol{\gamma}[k]$ in (14) is valid for the given parameters.

To confirm the validity of (18), a comparison of the RMSE performance is shown in Figure 11. Because it is difficult to theoretically obtain the original form of $\boldsymbol{V}_{\mathrm{ud}}[k]$, it is difficult to evaluate the approximation in (18) itself. Here, instead of computing the difference between the approximation and the original form, we show the validity of $\boldsymbol{V}_{\mathrm{ud}}[k]$ by comparing the performance with the case of perfect error detection. If the presented $\boldsymbol{V}_{\mathrm{ud}}[k]$ is valid, the effect of the undetected bit errors will be correctly reduced in the state observer, and the control performance will approach the performance for the case with no undetected error. In Figure 11, the graphs with filled circles and triangles are the same graphs as Figure 5. The graphs with open

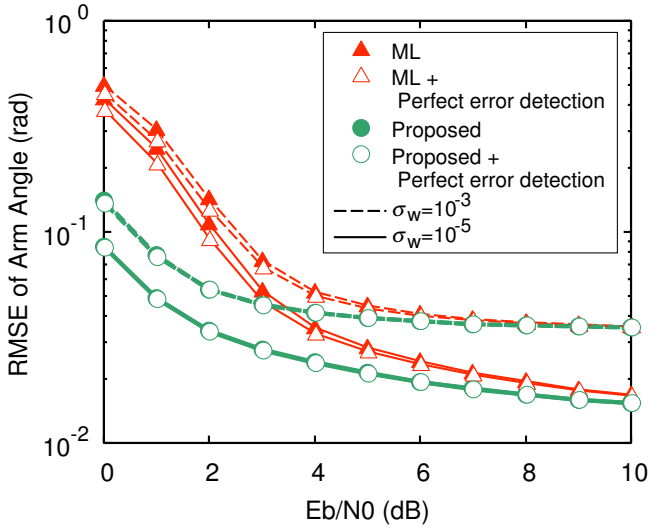

Fig. 11. Comparison with the case of perfect error detection

circles and triangles show the RMSE performance when error detection is perfect, i.e., there is no undetected error; therefore, $\boldsymbol{V}_{\mathrm{ud}}[k] = \mathbf{0}$. We can see that the RMSE performance of both the ML and proposed receivers with $\boldsymbol{V}_{\mathrm{ud}}[k]$ is nearly the same as the performance in the case with no undetected error. In particular, the occurrence of undetected bit errors becomes smaller for the proposed receiver because of the smaller error rate performance, as shown in Figure 4; thus, the performance degradation resulting from the approximation in (18) is negligible.

V. Conclusion and Discussion

We considered a cross-layer design for the optimized receiver for state feedback in wireless feedback control systems. The proposed receiver is based on an MAP decision in the communication layer but differs in that it is connected with a Kalman filter-based state observer in the control layer by a recursive structure. It utilizes the estimated state information of the state observer as à priori information and provides error covariance information for the state observer. We showed that the proposed receiver can effectively reduce the number of channel errors in the received state feedback and improve control performance, particularly at a low SNR. Our design is simple and quite suitable for a feedback control loop because it does not require any cost for calculating the à priori information. It has a structure similar to joint channel estimation and decoding, e.g., [34], [35], which exploit the implicit redundancy of the transmitted data by

a recursive structure in the communication layer; therefore, our recursive structure is similarly effective.

In this paper, the considered scenario was simplified to clarify our proposal. (a) A control system with a single plant was considered; however, even with multiple plants, the state-space representation of each controller–plant system or the total system can be represented in the same way as (1) and (2). As long as the state-space representation is applicable, our proposal is also applicable. (b) The channel matrix was assumed to be known at the receiver; however, if there is some uncertainty in the channel matrix, a performance degradation simply appears for both the ML and proposed receivers. As shown in (11) for the ML receiver and the first term of (15) for the proposed receiver, the contribution of the channel matrix for the proposed receiver is the same as that for the ML receiver. If an appropriate channel estimator such as a minimum mean square error estimator is used, the effect of the uncertainty in the channel matrix simply appears as a gentler PER curve. Moreover, the state observer does not depend on how the receiver works and depends only on whether the received packet is discarded. Therefore, the effect of the uncertainty in the channel matrix on the state observer has no special difference from the effect of the lower SNR. (c) A specific existing communication protocol was not considered; however, the system representation in [36], [37] is nearly the same as that described in this paper. Therefore, our proposal will be applicable to the IEEE 802.15.4 protocol. (d) An error correction code was not used; if used, it should be used as an outer code for error-detection-coded data rather than an error detection code. If an error correction code is used as an outer code, some improvement in performance will be obtained according to its error correction property; however, the improvement simply appears for both the ML and proposed receivers. In the case of convolutional, turbo, and low-density parity-check codes, there are efficient algorithms such as soft-output Viterbi, BCJR, and sum-product algorithms, for the computation of an MAP decision. Designing the proposed receiver to work with such efficient algorithms is planned for future work.

REFERENCES

[1] L. Zhang, H. Gao, and O. Kaynak, "Network-induced constraints in networked control systems – a survey," *IEEE Trans. Ind. Informat.*, vol. 9, no. 1, pp. 403–416, Feb. 2013.

[2] L. Li and Y. Xia, "Unscented Kalman filter over unreliable communication networks with Markovian packet dropouts," *IEEE Trans. Autom. Control*, vol. 58, no. 12, pp. 3224–3230, Dec. 2013.

[3] X. He, Z. Wang, X. Wang, and D. H. Zhou, "Networked strong tracking filtering with multiple packet dropouts: Algorithms and applications," *IEEE Trans. Ind. Electron.*, vol. 61, no. 3, pp. 1454–1463, Mar. 2014.

[4] E. R. Rohr, D. Marelli, and M. Fu, "Kalman filtering with intermittent observations: On the boundedness of the expected error covariance," *IEEE Trans. Autom. Control*, vol. 59, no. 10, pp. 2724–2738, Oct. 2014.

[5] L. Schenato, B. Sinopoli, M. Franceschetti, K. Poolla, and S. S. Sastry, "Foundations of control and estimation over lossy networks," *Proc. of the IEEE*, vol. 95, no. 1, pp. 163–187, Jan. 2007.

[6] M. Trivellato and N. Benvenuto, "State control in networked control systems under packet drops and limited transmission bandwidth," *IEEE Trans. Commun.*, vol. 58, no. 2, pp. 611–622, Feb. 2010.

[7] E. Garone, B. Sinopoli, A. Goldsmith, and A. Casavola, "LQG control for MIMO systems over multiple erasure channels with perfect acknowledgment," *IEEE Trans. Autom. Control*, vol. 57, no. 2, pp. 450–456, Feb. 2012.

[8] J. te Yu and L.-C. Fu, "An optimal compensation framework for linear quadratic Gaussian control over lossy networks," *IEEE Trans. Autom. Control*, vol. 60, no. 10, pp. 2692–2697, Oct. 2015.

[9] D. E. Quevedo and I. Jurado, "Stability of sequence-based control with random delays and dropouts," *IEEE Trans. Autom. Control*, vol. 59, no. 5, pp. 1296–1302, May 2014.

[10] H. Li and Y. Shi, "Network-based predictive control for constrained nonlinear systems with two-channel packet dropouts," *IEEE Trans. Ind. Electron.*, vol. 61, no. 3, pp. 1574–1582, Mar. 2014.

[11] Z.-H. Pang, G.-P. Liu, D. Zhou, and M. Chen, "Output tracking control for networked systems: A model-based prediction approach," *IEEE Trans. Ind. Electron.*, vol. 61, no. 9, pp. 4867–4877, Sep. 2014.

[12] W. Zhang, J. Bae, , and M. Tomizuka, "Modified preview control for a wireless tracking control system with packet loss," *IEEE/ASME Trans. Mechatronics*, vol. 20, no. 1, pp. 299–307, Feb. 2015.

[13] D. Wang, J. Wang, and W. Wang, "H_∞ controller design of networked control systems with Markov packet dropouts," *IEEE Trans. Syst., Man, Cybern., Syst.*, vol. 43, no. 3, pp. 689–697, May 2013.

[14] D. Zhang, Q.-G. Wang, L. Yu, and Q.-K. Shao, "H_∞ filtering for networked systems with multiple time-varying transmissions and random packet dropouts," *IEEE Trans. Ind. Informat.*, vol. 9, no. 3, pp. 1705–1716, Aug. 2013.

[15] Z. Du, D. Yue, and S. Hu, "H-infinity stabilization for singular networked cascade control systems with state delay and disturbance," *IEEE Trans. Ind. Informat.*, vol. 10, no. 2, pp. 882–894, May 2014.

[16] A. Ulusoy, O. Gurbuz, and A. Onat, "Wireless model-based predictive networked control system over cooperative wireless network," *IEEE Trans. Ind. Informat.*, vol. 7, no. 1, pp. 41–51, Feb. 2011.

[17] T. Futatsugi, C. Sugimoto, and R. Kohno, "A study on HARQ error-controlling scheme for the wireless control of medical equipment," in *Proc. 2012 6th Int. Symp. Medical Informat. and Commun. Technol. (ISMICT)*, Mar. 2012, pp. 1–4.

[18] H. Li, J. B. Song, and Q. Zeng, "Adaptive modulation in networked control systems with application in smart grids," *IEEE Commun. Lett.*, vol. 17, no. 7, pp. 1305–1308, Jul. 2013.

[19] K. Gatsis, A. Ribeiro, and G. J. Pappas, "Optimal power management in wireless control systems," *IEEE Trans. Autom. Control*, vol. 59, no. 6, pp. 1495–1510, Jun. 2014.

[20] S. Hattori, K. Kobayashi, H. Okada, and M. Katayama, "ON-OFF error control coding scheme for minimizing tracking error in wireless feedback control systems," *IEEE Trans. Ind. Informat.*, vol. 11, no. 6, pp. 1411–1421, Dec. 2015.

[21] Y. Miwa, K. Kobayashi, H. Okada, and M. Katayama, "A study on variable length channel coding for state feedback in wireless control systems," in *Proc. IEEE Wireless Commun. Netw. Conf. (WCNC)*, Mar. 2017.

[22] J. S. Freudenberg, R. H. Middleton, and J. H. Braslavsky, "Minimum variance control over a Gaussian communication channel," *IEEE Trans. Autom. Control*, vol. 56, no. 8, pp. 1751–1765, Aug. 2011.

[23] K. Eswaran and M. Gastpar, "Feedback communication and control over a single channel," *IEEE Trans. Inf. Theory*, vol. 59, no. 10, p. 6243, Oct. 2013.

[24] S. Dey, A. Chiuso, and L. Schenato, "Remote estimation with noisy measurements subject to packet loss and quantization noise," *IEEE Trans. Control Netw. Syst.*, vol. 1, no. 3, pp. 204–217, Sep. 2014.

[25] S. Gong, H. Li, L. Lai, and R. Qiu, "Decoding the 'nature encoded' messages for distributed energy generation control in microgrid," in *Proc. 2011 IEEE Int. Conf. Communications (ICC)*, Jun. 2011, pp. 1–5.

[26] S. Gong, "Decoding the 'nature encoded' messages for wireless networked control systems," Ph.D. dissertation, University of Tennessee, Knoxville, Dec. 2013. [Online]. Available: http://trace.tennessee.edu/utk_graddiss/2574/

[27] B. Farber and K. Zeger, "Quantizers with uniform encoders and channel optimized decoders," *IEEE Trans. Inf. Theory*, vol. 50, no. 1, pp. 62–77, Jan. 2004.

[28] I. Land, P. Hoeher, and U. Sorger., "Log-likelihood values and Monte Carlo simulation – some fundamental results," in *Proc. Int. Symp. on Turbo Codes & Rel. Topics*, Sep. 2000, pp. 43–46.

[29] A. J. Viterbi, "An intuitive justification and a simplified implementation of the MAP decoder for convolutional codes," *IEEE J. Sel. Areas Commun.*, vol. 16, no. 2, pp. 260–264, Feb. 1998.

[30] RealTEC, "RTC05," [Online]. Available: http:www011.upp.so-net.ne.jp/realtec/rtc05.pdf.

[31] T. S. Rappaport, "Indoor radio communications for factories of the future," *IEEE Commun. Mag.*, vol. 27, no. 5, pp. 15–24, May 1989.

[32] S.-C. Kim, H. L. Bertoni, and M. Stern, "Pulse propagation characteristics at 2.4 GHz inside buildings," *IEEE Trans. Veh. Technol.*, vol. 45, no. 3, pp. 579–592, Aug. 1996.

[33] P. Koopman, "Best CRC polynomials," [Online]. Available: http://users.ece.cmu.edu/~koopman/crc/.

[34] J. Mitra and L. Lampe, "On joint estimation and decoding for channels with noise memory," *IEEE Commun. Lett.*, vol. 13, no. 10, pp. 730–732, Oct. 2009.

[35] R. Prasad, C. R. Murthy, and B. D. Rao, "Joint channel estimation and data detection in MIMO-OFDM systems: A sparse Bayesian learning approach," *IEEE Trans. Signal Process.*, vol. 63, no. 20, pp. 5369–5382, Oct. 2015.

[36] E. G. W. Peters, D. E. Quevedo, and M. Fu, "Controller and scheduler codesign for feedback control over IEEE 802.15.4 networks," *IEEE Trans. Control Syst. Technol.*, vol. 24, no. 6, pp. 2016–2030, Nov. 2016.

[37] Y. Uematsu, K. Kobayashi, H. Okada, and M. Katayama, "A study on multiple access schemes for wireless control over the IEEE 802.15.4 beacon-enabled mode," in *Proc. IEEE Wireless Commun. Netw. Conf. (WCNC)*, Mar. 2017.

Kentaro Kobayashi was born in Mie, Japan, in 1983. He received the B.S., M.S. and Ph.D. degrees from Nagoya University, Nagoya, Japan, in 2005, 2007, and 2010, respectively, all in Electrical Engineering and Computer Science.

From 2009 to 2010, he was a Research Fellow of the Japan Society for the Promotion of Science with Nagoya University. Since 2010, he has been an Assistant Professor with Nagoya University. His research interests include cross-layer design and optimization of communication and control, wireless sensor networks, distributed detection, and distributed coding.

Dr. Kobayashi is a Member of The Institute of Electronics, Information and Communication Engineers (IEICE) and Information Processing Society of Japan (IPSJ). He was the recipient of the Young Researcher Award of 2009 from IEICE Technical Committee on Mobile Network and Applications (was Technical Committee on Mobile Multimedia Communications) and the IEICE Young Researcher's Award in 2013.

Hiraku Okada received the B.S., M.S. and Ph.D. degrees in Information Electronics Engineering from Nagoya University, Nagoya, Japan, in 1995, 1997, and 1999, respectively.

From 1997 to 2000, he was a Research Fellow of the Japan Society for the Promotion of Science with Nagoya University. He was an Assistant Professor with Nagoya University from 2000 to 2006; an Associate Professor with Niigata University, Niigata, Japan, from 2006 to 2009; and an Associate Professor with Saitama University, Saitama, Japan, from 2009 to 2011. Since 2011, he has been an Associate Professor with Nagoya University. His research interests include wireless communication systems, wireless networks, inter-vehicle communications, and visible light communication systems.

Dr. Okada is a Member of Association for Computing Machinery (ACM) and IEICE. He was the recipient of the Inose Science Award in 1996, the IEICE Young Engineer Award in 1998, and the IEICE Communications Express (ComEX) Best Letter Award in 2014.

Masaaki Katayama was born in Kyoto, Japan, in 1959. He received the B.S., M.S. and Ph.D. degrees from Osaka University, Osaka, Japan, in 1981, 1983, and 1986, respectively, all in Communication Engineering.

He was an Assistant Professor with Toyohashi University of Technology, Toyohashi, Japan, from 1986 to 1989, and a Lecturer with Osaka University from 1989 to 1992. In 1992, he joined Nagoya University, Nagoya, Japan, as an Associate Professor, and has been a Professor since July 2001. He was a Visiting Scholar at the College of Engineering, University of Michigan, Ann Arbor, MI, USA, from 1995 to 1996. His research interests include smart grid and energy management systems, wireless sensing and control, cognitive radio, power-line communications, visible light communications, next-generation mobile communications, and future satellite communications.

Dr. Katayama is a Fellow Member of the IEICE and a Member of Reliability Engineering Association of Japan. He was the recipient of the IEICE (was Institute of Electronics and Communication Engineering of Japan) Shinohara Memorial Young Engineer Award in 1986 and the 2012 Outstanding Service Award from IEEE Communications Society Technical Committee on Power Line Communications.